– Supplementary Information –

Surface Adsorbate Fluctuations and Noise in Nanoelectromechanical Systems

Y. T. Yang[†1], C. Callegari[†2], X. L. Feng[†3], M. L. Roukes[*]
Kavli Nanoscience Institute, Mail Code 114-36
California Institute of Technology, Pasadena, CA 91125, USA

This article provides supplementary information to the main text of the title manuscript. We present in Section I the experimental system and techniques employed, along with supporting experimental data. In Section II we present the supporting theoretical and modeling work.

[†] These authors contributed to this work equally.
[1] Present address: Department of Electrical Engineering, National Tsing-Hua University, Hsinchu, Taiwan 30013, R.O.C.
[2] Present address: Sincrotrone Trieste, Basovizza Trieste, Italy.
[3] Present address: Electrical Engineering, Case Western Reserve University, Cleveland, OH 44106, USA.
[*] Corresponding author. Email: roukes@caltech.edu

I. Experimental Techniques and Supporting Data

1. Experimental System and Apparatus

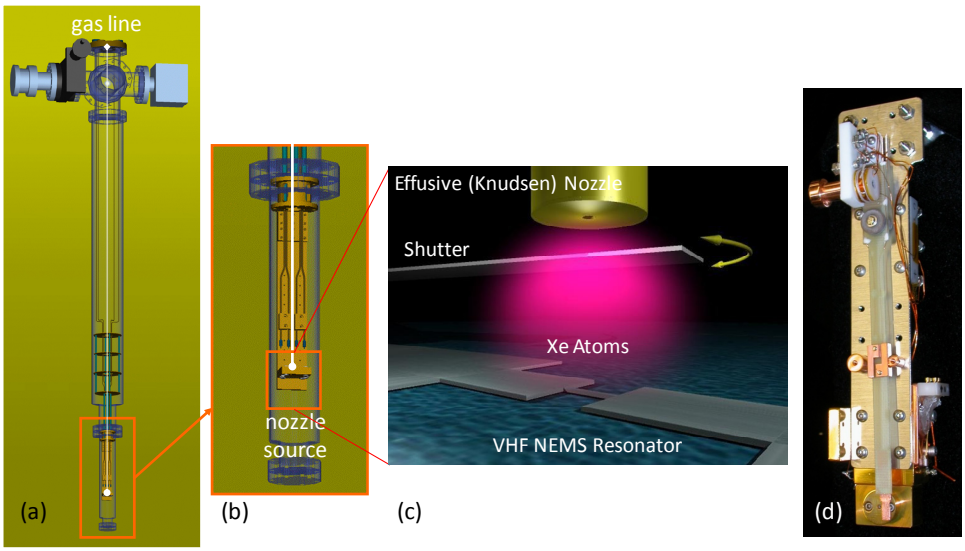

Figure S1. Experimental apparatus. (a) Illustration (design drawing) of the ultra high vacuum (UHV) cryostat with various feedthroughs including very high and ultra high frequency (VHF/UHF) electronics and a gas delivery line. (b) Close-up view of the sample stage area, with VHF/UHF electronic connections, and micronozzle structure. (c) Illustration of the basic principle of the experiment, with the shutter-regulated micronozzle impinging Xe atoms toward the surface of a vibrating VHF NEMS resonator. (d) A picture of the gas nozzle-shutter assembly employed in this work.

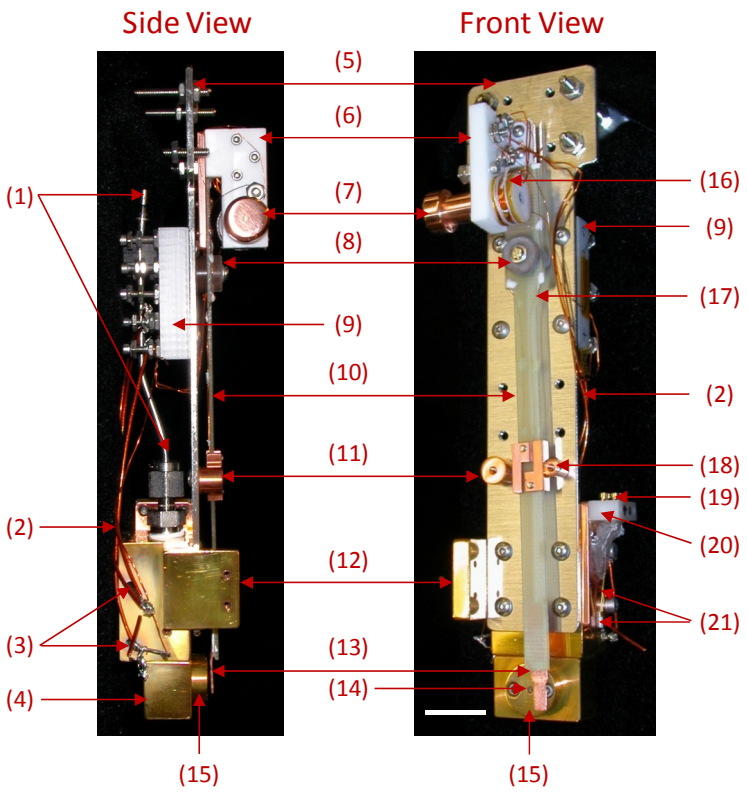

Figure S2. The gas nozzle-shutter assembly. (1) Gas line (stainless steel gas tube, outside diameter 1/16", inside diameter 1/32") going to the micronozzle. This supplies the Xe gas flux from the buffer chamber (upstream and outside of the UHV cryostat chamber) to the gas nozzle. (2) Wires for heaters. (3) Mounting holes for heaters. The heaters are resistors, which are wired up and connected to a temperature controller (LakeShore 331, outside of the UHV chamber) for stabilizing the gas nozzle chamber temperature at 200K. (4) Micronozzle gas chamber (gold plated brass). (5) Base/backbone plate (stainless steel). (6) Insulating (Delrin) mounting block for the coil and contacts, and for the counter balance. (7) Counter balance (brass mass). (8) Pivot for the swing arm. (9) Insulating (Delrin) block for contacts and wires. (10) Swing arm (G10 plastic). (11) Close sensing contact (copper-copper). (12) Main gas chamber and house for heaters [gold plated brass, fit and sealed to (4)]. The connection between this main gas chamber block to the base plate (5) has been made via 4 pads with small contact surface, to limit the unnecessary heat transfer to the base plate. (13) Shutter. (14) Micronozzle aperture. (15) Nozzle disk [fit and sealed to (4), disks were made available with different aperture sizes, and we tested disks with aperture diameters of 30, 100, and 300μm]. (16) Coil for electromagnetic actuation of the shutter. The nozzle-shutter assembly is vertically mounted in the UHV cryostat in a strong vertical magnetic field; a small amount of electrical current applied to this coil induces a horizontal magnetic field, hence the electromagnetic actuation and deflection of the swing arm (10) with respect to the pivot (8). (17) Thin wires for sensing contacts. (18) Open sensing contact (copper-copper). (19) Pins for feedthrough wiring of heater and thermometer. (20) Insulating (Delrin) block for contacts and pins. (21) Diode thermometer (LakeShore DT-470) and wires. The scale bar is 1cm.

2. NEMS Resonance Readout

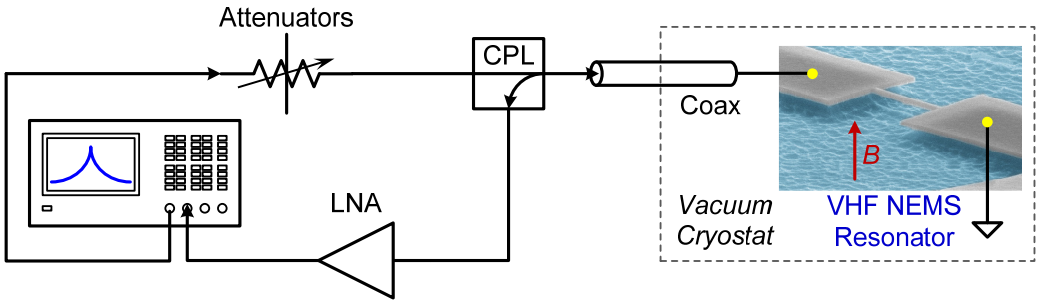

Figure S3. Schematic of the open-loop VHF NEMS resonance signal transduction scheme. The VHF NEMS resonance excitation and detection of electromechanical response are based on magnetomotive transduction in a strong magnetic field (*B*). The two-port measurement uses a HF/VHF network analyzer (HP3577A). The readout circuit is a reflectrometry scheme using a directional coupler (CPL) and a low-noise amplifier (LNA).

3. Real-Time Resonance Frequency Locking and Tracking, and the Noise Measurements

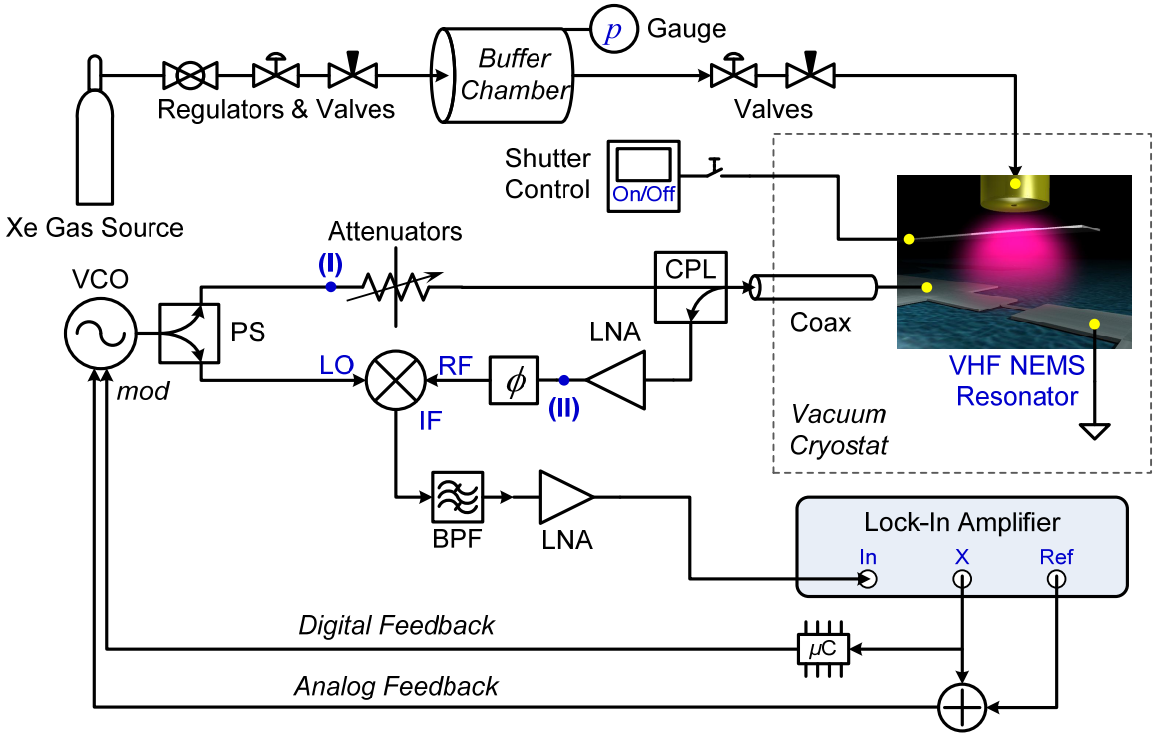

Figure S4. Diagram of the experimental setup and the measurement system. The gas delivery sub-system include Xe gas source (lecture bottle cylinder), a buffer chamber and a specialized gas feedthrough line leading to the micro-nozzle which is positioned and aligned in the vicinity of the NEMS device; it also includes various accessories such

as pressure gauges, regulators, and various coarse and fine tuning control valves. The electromechanical shutter is controlled by a relay circuit. For real-time resonance frequency locking and tracking, the NEMS resonance readout circuit (described in Figure S2) is embedded into a closed loop with feedback, which consists of a frequency-modulation phase-locked loop (FM-PLL).[1] VCO: voltage controlled oscillator, BPF: band-pass filter. As shown, time-domain frequency instability is measured by using a high-precision frequency counter. Noise spectra are measured by using a dynamical signal and noise analyzer. Also, as shown in Figure S2, nodes (I) and (II) here in Figure S3 indicate the alternative configuration for switching back to the open-loop resonance detection circuit.

4. Temperature-Programmed Adsorption (TPA)

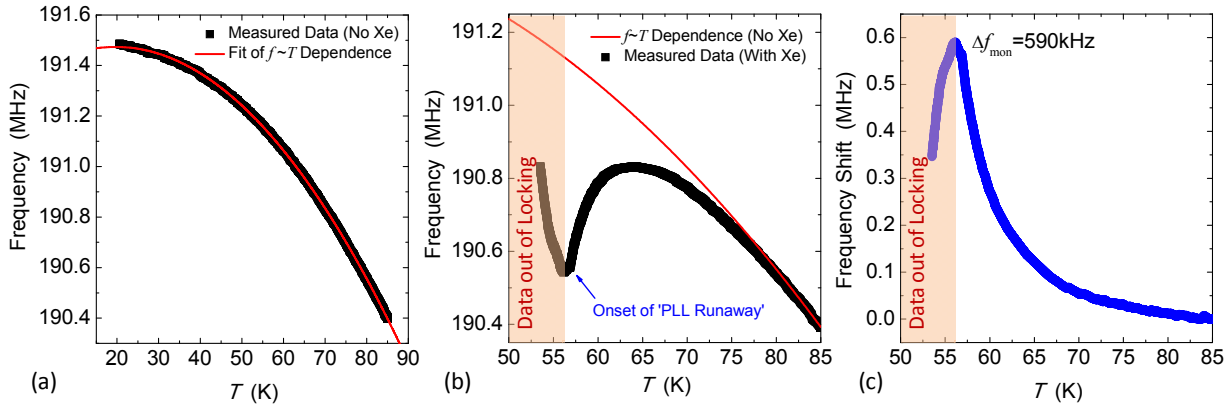

Figure S5. A typical set of measured data for the demonstration of temperature-programmed adsorption (TPA). (a) A fresh measurement of resonance frequency as a function of device temperature when there is no impingement of Xe gas at all. This measurement gives a baseline $f \sim T$ dependence as shown by the fit to the data. (b) Measured frequency trace raw data when there is impingement of Xe gas flux and hence temperature-programmed adsorption. The raw data of measured resonance frequency tracked by the FM-PLL is plotted together with the previously calibrated $f \sim T$ dependence. Here the measured f as a function of T is due to both the pure temperature dependence and the loading of surface adsorbates (Xe atoms). Note the onset of the 'PLL runaway' near $T \approx 56$K. Beyond this point, the data trace in the lower temperature range is out of lock and not meaningful. In fact, each time this happens, we heat up the device to restore to the fresh surface condition. The Xe gas flux is stopped. We switch to the open-loop resonance detection circuit scheme (Figure S3) with network analyzer to find the NEMS resonance signal again, and we manually bring the FM-PLL back into lock.

5. *Q* Factor Temperature Dependence

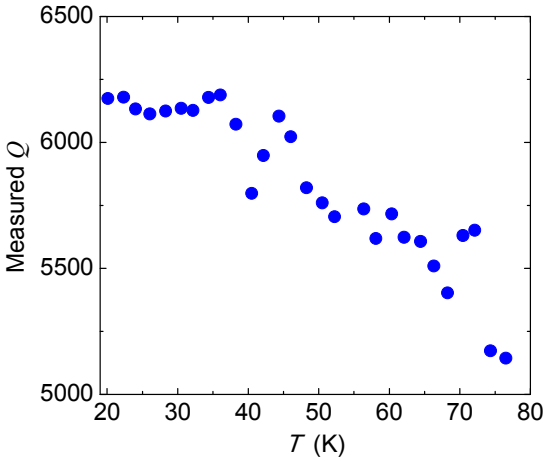

Figure S6. Measured device quality factor (Q) as a function of device temperature. No Xe gas impingement in this measurement. There is a mild but steady Q increase as T is decreased in the range of 20~80K. A similar tendency has also been observed in other VHF/UHF NEMS resonators.[2] Here this measurement verifies the weak temperature dependence of Q. This is also in good qualitative consistence with the observed mild reduction of frequency instability (noise floor without Xe gas flux) as the temperature is decreased (see Figure 3 in main text), because theoretically the frequency instability should be proportional to the inverse of Q.[3]

II. Theoretical Analyses and Modeling

1. Noise due to Surface Diffusion

Here we describe our treatment of the noise process due to adsorbates diffusion on the surface of NEMS device.

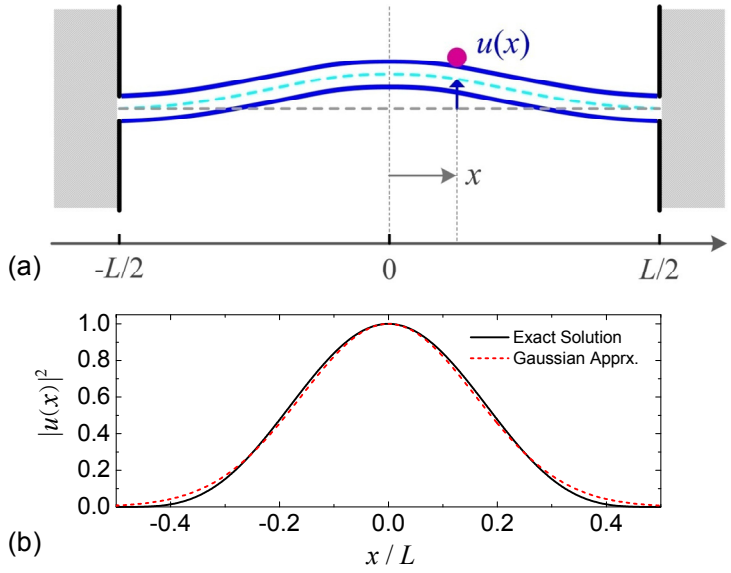

Figure S7. (a) Schematic illustration of mode-shape and location-dependent mass loading response for a doubly clamped beam. (b) The square of normalized mode shape and its optimized Gaussian approximation.

For the doubly clamped beam NEMS resonator operating in its fundamental flexural mode, we first consider its mode shape and the position-dependent frequency shift induced by mass loading effect of an adsorbed atom. As illustrated in Figure S7, the *normalized* mode shape is

$$u(x) = 0.8827\cos kx + 0.1173\cosh kx\,, \tag{S1}$$

for $x\in[-L/2,\ L/2]$, with $u(0)=1$, $k=4.73/L$ and L being the beam length.[4] For our interest in developing an analytic approach, we have found that approximating the square of the normalized mode shape $[u(x)]^2$ with a Gaussian function and extending the integration interval from $[-L/2,\ L/2]$ to $(-\infty,\ \infty)$ considerably simplifies the calculations we present here. Minimizing the 'distance' norm between the two functions by means of a least square technique, we have found

an excellent approximation $[u(x)]^2 = \exp\left[-(ax/L)^2\right]$ (see Figure S10) with an optimized parameter a=4.42844.

When an atom (or molecule) of mass m lands at position x on the surface of device (with total mass M), and assuming the added mass only changes the kinetic energy but not the potential (flexural) energy of the device, we have the fractional frequency variation (with respect to the initial reference frequency f_0 or ω_0),

$$\frac{\delta f}{f_0} = \frac{\delta\omega}{\omega_0} = -\frac{1}{2}\frac{m}{M}\frac{|u(x)|^2}{\frac{1}{L}\int_{-L/2}^{L/2}[u(x)]^2\,dx} \approx -\frac{1}{2}\frac{m}{M_{eff}}|u(x)|^2 . \tag{S2}$$

Here we have $M_{eff} = M\cdot\frac{1}{L}\int_{-L/2}^{L/2}[u(x)]^2\,dx \approx \frac{\sqrt{\pi}}{a}M$, which yields the effective modal mass $M_{eff} = 0.40M$. (The effective mass is $0.397M$ if we use the original solution, confirming that the Gaussian approximation is excellent with discrepancy <1%). For a quasi-continuous distribution of adsorbates mass over the length of the NEMS device, we can simply replace $m\cdot|u(x)|^2$ with $mC(x)\cdot|u(x)|^2$, with $C(x)$ being the concentration of the adsorbed atoms (number density per unit length).

We consider pure diffusion of one species in one dimension. The concentration fluctuation $\delta C(x,t)$ obeys the following diffusion equation,

$$\frac{\partial\delta C(x,t)}{\partial t} = D\frac{\partial^2\delta C(x,t)}{\partial x^2} . \tag{S3}$$

The Fourier transform $\mathcal{F}_k[\delta C(x,t)] = \tilde{C}(k,t)$ obeys

$$\frac{\partial\tilde{C}(k,t)}{\partial t} = -Dk^2\tilde{C}(k,t), \tag{S4}$$

and hence

$$\tilde{C}(k,t) = e^{-Dk^2t}\tilde{C}(k,0), \tag{S5}$$

where k is the wave number.

The device frequency fluctuation due to the mass fluctuation is given by

$$y(t) \equiv \frac{\delta f(t)}{f_0} = -\frac{1}{2}\frac{m}{M}\frac{\int_{-L/2}^{L/2}[u(x)]^2\,\delta C(x,t)dx}{\frac{1}{L}\int_{-L/2}^{L/2}[u(x)]^2\,dx} \approx -\frac{1}{2}\frac{a}{\sqrt{\pi}}\frac{m}{M}\int_{-L/2}^{L/2}\delta C(x,t)[u(x)]^2\,dx\,. \qquad \text{(S6)}$$

We can now calculate the autocorrelation function of the fractional frequency fluctuations due to surface diffusion,

$$\begin{aligned} G(\tau) &= \frac{\langle \delta f(t)\cdot \delta f(t+\tau)\rangle}{f_0^{\,2}} \\ &= \left(\frac{m}{2M}\right)^2 \frac{a^2}{\pi}\int_{-L/2}^{L/2}dx\int_{-L/2}^{L/2}u^2(x)u^2(x')\langle \delta C(x,t+\tau)\cdot \delta C(x',t)\rangle dx', \qquad \text{(S7)} \\ &= \left(\frac{m}{2M}\right)^2 \frac{a^2}{\pi}\int_{-L/2}^{L/2}dx\int_{-L/2}^{L/2}u^2(x)u^2(x')\phi(x,x',\tau)dx' \end{aligned}$$

where $\phi(x,x',\tau) = \langle \delta C(x,t+\tau)\cdot \delta C(x',t)\rangle$.

Employing Fourier transform techniques (recall the classical application of Fourier transform and its properties to solving diffusion-type differential equations),[5] we calculate and carry out transforms explicitly to yield

$$\phi(x,x',\tau) = \frac{N}{L}\frac{1}{2\sqrt{\pi D\tau}}\exp\left[-\frac{(x-x')^2}{4D\tau}\right], \qquad \text{(S8)}$$

in which N is the average total number of adsorbed atoms on the device surface. Further, we use the above result for $\phi(x,x',\tau)$ to calculate the double integral in Eq. (S7), again with the integration limits extended to (–∞, ∞), and we obtain[6]

$$G(\tau) = NL\left(\frac{m}{2M}\right)^2 \frac{a}{\sqrt{\pi}} \frac{1}{\sqrt{2L^2 + 4a^2 D\tau}} = \frac{aN}{\sqrt{2\pi}}\left(\frac{m}{2M}\right)^2 \frac{1}{\sqrt{1+\tau/\tau_D}} \tag{S9}$$

where we define the characteristic diffusion time $\tau_D = L^2/(2a^2 D)$. The advantage of being able to carry out analytically the calculation of the autocorrelation function well justifies the Gaussian approximation of the mode shape. It is interesting and worth noting that $G(\tau)$ is of the form $(1+\tau/\tau_D)^{-d/2}$ with d=1, the dimensionality of the problem in the present study. In fact, we note that our analysis here is in good analogy to the well-known theory of fluorescence correlation spectroscopy (FCS),[7,8] in which the correlation function scales as $(1+\tau/\tau_D)^{-1}$, consistent with the dimension (d=2) of the FCS process.

Now we employ the Wiener-Khinchin theorem[9] to obtain the corresponding double-sided (DS) spectral density of fractional frequency noise,

$$\begin{aligned} S_{y,DS}(\omega) &= \int_{-\infty}^{\infty} G(\tau) e^{-i\omega\tau} d\tau = \int_{-\infty}^{\infty} G(\tau)\cos(\omega\tau) d\tau \\ &= aN\left(\frac{m}{2M}\right)^2 \sqrt{\frac{2}{\pi}} \cdot \int_0^{\infty} \frac{\cos(\omega\tau)}{\sqrt{1+\tau/\tau_D}} d\tau \\ &= aN\left(\frac{m}{2M}\right)^2 \sqrt{\frac{2}{\pi}} \cdot \left[\sqrt{\frac{\pi}{2}} \cdot \tau_D \frac{g\left(\sqrt{\omega\tau_D}\right)}{\sqrt{\omega\tau_D}}\right] \\ &= \frac{aN}{4}\left(\frac{m}{M}\right)^2 \cdot \left[\tau_D \xi(\omega\tau_D)\right] \end{aligned} \tag{S10a}$$

The more useful single-sided (SS) spectral density (folding the negative Fourier frequency part over onto the positive side, corresponding to practical measurements)[10,11] is thus

$$S_y(\omega) = 2S_{y,DS}(\omega) = \frac{aN}{2}\left(\frac{m}{M}\right)^2 \cdot \left[\tau_D \xi(\omega\tau_D)\right]. \tag{S10b}$$

In the above calculation the integral for a combined trigonometric-algebraic function[6] leads to $\xi(x) \equiv \frac{g(\sqrt{x})}{\sqrt{x}}$, $g(\sqrt{x}) = \cos(x) + \sin(x) - 2C_1(\sqrt{x})\cos(x) - 2S_1(\sqrt{x})\sin(x)$; with $C_1(x)$ and $S_1(x)$ the Fresnel integrals,[3] defined by

$$C_1(x) = \sqrt{\frac{2}{\pi}} \int_0^x \cos(u^2) du \,, \tag{S11a}$$

$$S_1(x) = \sqrt{\frac{2}{\pi}} \int_0^x \sin(u^2) du \,. \tag{S11b}$$

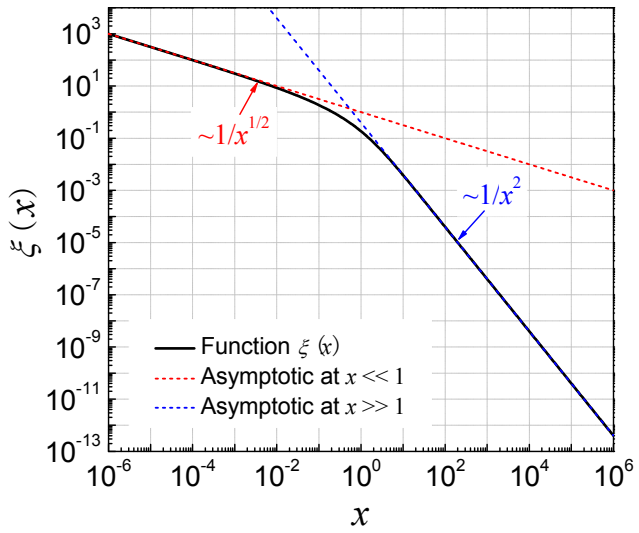

Figure S8. Plot of the function $\xi(x)$ with its asymptotic functions: (i) $x^{-1/2}$ for $x<<1$, and (ii) $(2\pi)^{-1/2}x^{-2}$ for $x>>1$.

There exist two asymptotic functions of particular interest for the $\xi(x)$ in the spectral density: (i) for $x << 1$, $\xi(x) \approx 1/\sqrt{x}$; and (ii) for $x >> 1$, $\xi(x) \approx \frac{1}{\sqrt{2\pi} \cdot x^2}$. In Figure S8 we plot the function $\xi(x) \equiv \frac{g(\sqrt{x})}{\sqrt{x}}$ and its asymptotic approximations. These lead to the following results:

(i) For $\omega << 1/\tau_D$ (*i.e.*, $\omega\tau_D << 1$), the spectral density of fractional frequency fluctuations is

$$S_y(\omega) = \frac{aN}{2}\left(\frac{m}{M}\right)^2 \sqrt{\frac{\tau_D}{\omega}}\,. \tag{S12}$$

(ii) For $\omega >> 1/\tau_D$ (*i.e.*, $\omega\tau_D >> 1$), the spectral density is

$$S_y(\omega) = \frac{aN}{2\sqrt{2\pi}}\left(\frac{m}{M}\right)^2 \frac{1}{\omega^2\tau_D}\,. \tag{S13}$$

Here we shall clarify and reiterate that these are the *excess* fractional frequency fluctuations spectral densities due to surface adsorbate diffusion. These excess spectral densities are thus additive to other uncorrelated noise spectral densities.

We now turn to discuss the modeling of the time-domain frequency instability. We can convert from the fractional frequency fluctuations spectral density to the frequency instability, Allan *variance*, as follows,[12,13]

$$\sigma_A^2(\tau_A) = \frac{4}{\pi}\int_0^\infty \frac{\sin^4(\omega\tau_A/2)}{(\omega\tau_A)^2} S_y(\omega)d\omega\,. \tag{S14}$$

Here τ_A is the averaging time and again $S_y(\omega)$ is the single-sided spectral density. τ_A is a characteristic time scale in practical measurements. Specifically, in our time-domain frequency stability measurements, τ_A is the time interval during which each averaged frequency data sample is acquired by the frequency counter. The integral essentially takes all the sideband noise contribution, with an equivalent frequency-domain transfer function set by τ_A. Depending on the time scales and employing the asymptotic functions of $S_y(\omega)$, we have the following cases with interesting power-law relationships:

(i) In the limit of slow measurement, $\tau_A >> \tau_D$ ($\omega\tau_D << \omega\tau_A$), the noise spectrum is dominated by the small-*x* asymptotic function $\xi(x) \equiv g\left(\sqrt{x}\right)\Big/\sqrt{x} = 1/\sqrt{x}$ and Eq. (S12), hence

$$\sigma_A^2(\tau_A) = \frac{2aN}{\pi}\left(\frac{m}{M}\right)^2\left(\frac{\tau_D}{\tau_A}\right)^{\frac{1}{2}} \cdot \int_0^\infty \frac{\sin^4(\omega\tau_A/2)}{(\omega\tau_A)^2}\sqrt{\frac{1}{\omega\tau_A}}d(\omega\tau_A), \tag{S15a}$$

By computing the Fresnel integrals, this yields the Allan *variance*

$$\sigma_A^2(\tau_A) \approx 0.6899 \cdot N\left(\frac{m}{M}\right)^2\left(\frac{\tau_D}{\tau_A}\right)^{\frac{1}{2}}, \tag{S15b}$$

and the Allan *deviation*

$$\sigma_A(\tau_A) \approx 0.83 \cdot \sqrt{N}\left(\frac{m}{M}\right)\left(\frac{\tau_D}{\tau_A}\right)^{\frac{1}{4}}. \tag{S15c}$$

(ii) In the limit of very fast measurement, $\tau_A << \tau_D$ ($\omega\tau_D >> \omega\tau_A$), and the noise spectrum is dominated by the large-x asymptotic $\xi(x) \equiv g\left(\sqrt{x}\right)/\sqrt{x} = 1/\left(\sqrt{2\pi}x^2\right)$, and with Eq. (S13), thus we have

$$\sigma_A^2(\tau_A) \approx 0.2610 \cdot N\left(\frac{m}{M}\right)^2\left(\frac{\tau_A}{\tau_D}\right), \tag{S16a}$$

$$\sigma_A(\tau_A) \approx 0.51 \cdot \sqrt{N}\left(\frac{m}{M}\right)\left(\frac{\tau_A}{\tau_D}\right)^{\frac{1}{2}} \tag{S16b}$$

In brief summary, we have two major observations here. First, the Allan deviation is proportional to $\sqrt{N}$ (N=$N(T)$ is the number of atoms on surface, measured as a function of temperature T) and mass ratio (m/M). Second, in different regimes the Allan deviation exhibits distinct approximate power-law dependences $(\tau_A/\tau_D)^\beta$ with $\beta = -1/4$, and $1/2$.

Most interesting and important, in the regime of $\omega\tau_D << 1$, the noise spectrum of fractional frequency fluctuation, $S_y(\omega)$, due to one-dimensional diffusion of adsorbates on surface, has power law $S_y(\omega) \sim \omega^\alpha$ with $\alpha = -1/2$ and correspondingly a frequency instability that scales as

$(\tau_A/\tau_D)^{\beta}$ with $\beta = -1/4$. These power laws are new; they represent the revelation of a new noise process that may become noticeable and important in NEMS resonators and oscillators, and possibly other low-dimension systems. In fact, as we examine the phase noise and frequency stability in various conventional oscillators or clocks (especially those based on electromechanical resonators), the known noise processes are thus far limited to power laws with α in integers (α= 0, ±1, ±2) and β as low as ±1/2.[14] In the conventional much bulkier, macroscopic electromechanical resonators, the subtlety of surface diffusion noise processes and the relatively weak power laws (α =–1/2 and β =–1/4) are simply not captured due to the device size and often the dominance of other noise processes (those with stronger power laws).

Our measurements of the Allan deviation are in regime (i) as described by Eq. (S15), as also discussed in the main text. We note that Allan variance given by Eqs. (S15)-(S18) is the *excess* variance due to the modeled surface diffusion process. The total frequency instability is thus $\sigma^2_{A,total}(\tau_A) = \sigma^2_{A,no-gas}(\tau_A) + \sigma^2_A(\tau_A)$ or $\sigma_{A,total}(\tau_A) = \sqrt{\sigma^2_{A,no-gas}(\tau_A) + \sigma^2_A(\tau_A)}$.

2. Noise due to Adsorption-Desorption

Here we describe the non-diffusive, pure adsorption-desorption model for surface adsorbates in the sub-monolayer regime. The surface is assumed to be saturated at the completion of the first monolayer, or implicitly equivalent, the atom-atom interaction is assumed to be much weaker than the atom-surface interaction so that only one monolayer can be accommodated. Non-diffusive means the adsorbates are laterally immobile on the surface. These conditions are essentially the same as in the analysis performed by Yong and Vig in dealing with adsorptive-desorptive contaminates on double-side surfaces of quartz crystal resonators.[15]

We consider a NEMS device with area A_D exposed to a constant impinging flux I for the incoming gas atoms (here I has the unit of number of atoms per unit area per sec). The number of available adsorption sites on the surface is N_a (ideally $N_a=A_D/A_{ad}$, with A_{ad} the area an adsorbate atom would occupy). The adsorption rate (number of atoms/sec) for the whole exposed area on the device is sIA_D, where s is the sticking probability or sticking coefficient for an incoming atom. Hence for each adsorption site the adsorption rate (in 1/sec, or Hz) is

$$r_{ad} = sI \cdot \frac{A_D}{N_a}. \tag{S19}$$

Each adsorption site can only accommodate a single atom. Once bound on the surface, the atom may attempt to leave the surface only by desorption (no diffusion). The desorption rate at each site (in Hz) is

$$r_{des} = v_{des} \exp\left(-\frac{E_{des}}{k_B T}\right). \tag{S20}$$

Here v_{des} is the attempt frequency, and E_{des} is the desorption energy or binding energy, which is the energy the atom is required to gain in order to get free from its adsorption site. When we have N ($N \le N_a$) atoms on the surface, the rate of atom desorption is $r_{des}N$. At the same time, there are (N_a–N) available adsorption sites (again, each adsorption site only accommodates one atom), and the rate of atoms being adsorbed is $r_{ad}(N_a - N)$. Therefore, at a given temperature

with a surface number coverage N, the steady-state balance is $r_{ad}\left(N_a - N\right) = r_{des}N$, which leads to

$$N = \frac{r_{ad}}{r_{ad} + r_{des}} N_a \,. \tag{S21}$$

As we only consider one species of adsorbates and one type of adsorption site, we define an empirical single correlation time τ_r of the adsorption-desorption cycle, $\tau_r = 1/\left(r_{ad} + r_{des}\right)$, which is essentially the Mathiessen's rule.[16] Hence from Eqs. (S19) and (S21), we have $\tau_r = N/\left(sIA_D\right)$.

Assume that the adsorption-desorption induced frequency change on each site is constant, $\delta\omega = -\left(m/2M\right)\omega_0$. By examining the frequency variations due to the Bernoulli-type stochastic process associated with each site and the whole ensemble,[15] we obtain the variance of the frequency fluctuation due to adsorption-desorption,

$$\sigma^2 = \frac{r_{ad}r_{des}}{\left(r_{ad} + r_{des}\right)^2}\left(\delta\omega\right)^2 N_a = \sigma_{occ}^2\left(\delta\omega\right)^2 N_a \,, \tag{S22a}$$

with

$$\sigma_{occ}^2 \equiv \frac{r_{ad}r_{des}}{\left(r_{ad} + r_{des}\right)^2} = \frac{N\left(N_a - N\right)}{{N_a}^2} \,, \tag{S22b}$$

which we define as the occupation variance. It is evident that the occupation variance assumes its maximum $\sigma_{occ}^2 = 1/2$ when $N = N_a/2$ (*i.e.*, at half coverage); and it vanishes at both N=0 and N=N_a (*i.e.*, zero coverage and completion of one monolayer, respectively). As N and the coverage are generally functions of temperature and pressure, so is the occupation variance. Similar to Yong and Vig[15], the autocorrelation function of frequency fluctuations induced by the adsorption-desorption is

$$G_{ad-des}\left(\tau\right) = \sigma^2 \exp\left(-\left|\tau\right|/\tau_r\right). \tag{S23}$$

The fractional frequency fluctuations spectrum is thus (again using Wiener-Khinchin theorem)

$$S_y(\omega)=\frac{2\sigma_{occ}^2 N_a \tau_r}{1+(\omega\tau_r)^2}\left(\frac{m}{2M}\right)^2. \tag{S24}$$

The excess Allan variance due to adsorption-desorption noise is (similar to Eq. (S14))

$$\sigma_A^2(\tau_A)=\frac{2}{\pi}\sigma_{occ}^2 N_a\left(\frac{m}{M}\right)^2 \tau_r \int_0^\infty \frac{\sin^4(\omega\tau_A/2)}{(\omega\tau_A)^2}\cdot\frac{1}{1+(\omega\tau_r)^2}d\omega, \tag{S25}$$

We analyze and obtain the following cases:

(i) In the limit of $\tau_A >> \tau_r$ ($\omega\tau_r << 1$), we have

$$\sigma_A^2(\tau_A)=\frac{1}{4}\sigma_{occ}^2 N_a\left(\frac{m}{M}\right)^2\frac{\tau_r}{\tau_A}, \tag{S26a}$$

$$\sigma_A(\tau_A)=\frac{1}{2}\sigma_{occ}\sqrt{N_a}\left(\frac{m}{M}\right)\left(\frac{\tau_r}{\tau_A}\right)^{\frac{1}{2}}. \tag{S26b}$$

(ii) In the limit of $\tau_A << \tau_r$ ($\omega\tau_r >> 1$), we have

$$\sigma_A^2(\tau_A)=\frac{1}{12}\sigma_{occ}^2 N_a\left(\frac{m}{M}\right)^2\frac{\tau_A}{\tau_r} \tag{S27a}$$

$$\sigma_A(\tau_A)=\frac{1}{2\sqrt{3}}\sigma_{occ}\sqrt{N_a}\left(\frac{m}{M}\right)\left(\frac{\tau_A}{\tau_r}\right)^{\frac{1}{2}}. \tag{S27b}$$

We see that in all cases the excess Allan deviation is proportional to the occupation deviation σ_{occ}, the square root of total number of sites N_a, and the mass ratio (m/M). In slow measurements (averaging time considerably longer than the characteristic time of the adsorption-desorption process), the Allan deviation scales with $1/\sqrt{\tau_A}$, similar to that of a thermal noise dominated process. If the measurements can be done much faster than the atoms' adsorption-desorption cycles, the instability will scale with $\sqrt{\tau_A}$, as in the case dominated by random-walk

frequency modulations.[14] Of course, in all cases, the occupation variance σ_{occ} takes into account the effects of the physical parameters (*e.g.*, temperature, pressure, *etc.*) upon the surface.

Note we have assumed that the amount of frequency change due to adsorption-desorption event on each site is constant. If we consider the position dependency due to the mode shape, we ought to convert the picture of two-dimensional discrete adsorption sites to accommodate the one-dimensional continuous mode shape. We can define the adsorption site density per unit length, N_a/L, and integrate over the beam length to calculate the frequency fluctuation variance $\sigma^2 = \sigma_{occ}^2 \omega_0^2 \int_{-L/2}^{L/2} (N_a/L)(m/2M)^2 |u(x)|^4 dx$, and hence the variance in Eq. (S21a), and Eqs. (S24)–(S27) should be corrected by a numerical factor of $1/L \int_{-L/2}^{L/2} (m/2M)^2 |u(x)|^4 dx \approx 0.29$ (and a factor of 0.54 for the Allan deviation).

References

[1] Yang, Y.T., Callegari, C., Feng, X.L., Ekinci, K.L., Roukes, M.L. *Nano Lett.* **6**, 583-586 (2006); Yang, Y.T., *Ph.D. Thesis*, California Institute of Technology (2006).

[2] Huang, X.M.H., Feng, X.L., Zorman, C.A., Mehregany, M., Roukes, M.L. *New J. Phys.* **7**, Art. No. 247 (2005); Feng, X.L., Zorman, C.A., Mehregany, M., Roukes, M.L. *Tech. Digest, The 12th Solid-State Sensors, Actuators and Microsystems Workshop (Hilton Head'06)*, pp. 86-89 (2006); Hutchinson, A.B., Truitt, P.A., Schwab, K.C., Sekaric, L., Parpia, J.M., Craighead, H.G., Butler, J.E., *Appl. Phys. Lett.* **84**, 972-974 (2004); Mohanty, P., Harrington, D.A., Ekinci, K.L., Yang, Y.T., Murphy, M.J., Roukes, M.L. *Phys. Rev. B* **66**, 085416 (2002).

[3] Cleland, A.N., Roukes, M.L., *J. Appl. Phys.* **92**, 2758-2769 (2002).

[4] S. Timoshenko, D.H. Young, W. Weaver Jr, *Vibrational Problems in Engineering*, 4th Ed., New York: Wiley, Chapter 5 (1974).

[5] J. Mathews, R.L. Walker, *Mathematical Methods of Physics*, 2nd Ed., New York: Addison-Wesley, Chapter 4,8 (1971); E. Kreyszig, *Advanced Engineering Mathematics*, 9th Ed., New York: Jon Wiley & Sons, Chapter 12 (2006).

[6] I.S. Gradshteyn, I.M. Ryzhik (Edited by A. Jeffrey, D. Zwillinger), *Table of Integrals, Series and Products*, 7th Ed., Amsterdam: Elsevier (2007).

[7] D. Magde, E.L. Elson, W.W. Webb, *Phys. Rev. Lett.* **29**, 705-708 (1972).

[8] E.L. Elson, D. Magde, *Biopolymers* **13**, 1-27 (1974).

[9] C.W. Helstrom, *Statistical Theory of Signal Detection*, 2nd Ed., Oxford: Pergamon Press, Chapter 2 (1968); C. W. Helstrom, Probability and Stochastic Processes for Engineers, 2nd. Ed., New York: Macmillan, Chapter 6 (1991).

[10] R.K. Pathria, *Statistical Mechanics*, 2nd Ed., Oxford: Butterworth-Heinemann, Chapter 14 (1996); R.D. Blandford, K.S. Thorne, *Application of Classical Physics*, Caltech Textbook, Chapter 5 (2008).

[11] J. Rutman, *Proc. IEEE* **66**, 1048-1075 (1978).

[12] D. Allan, *Proc. IEEE* **54**, 221-230 (1966).

[13] W.F. Egan, *Frequency Synthesis by Phase Lock*, 2nd Ed., New York: John Wiley & Sons, Chapter 11 (2000).

[14] D.B. Sullivan, D.W. Allan, D.A. Howe, F.L. Walls (Eds.), *Characterization of Clocks and Oscillators* (NIST Technical Note 1337), Washington: US Government Printing Office (1990); and, *IEEE Standard 1139-1999*, New York, IEEE Press (1999).

[15] Y.K. Yong, J.R. Vig, *IEEE Trans. Ultrason. Ferroelect. & Freq. Contr.* **36**, 452-458 (1989); and *ibid*, **37**, 543-550 (1990).

[16] N.W. Ashcroft, N.D. Mermin, *Solid State Physics*, New York: Saunders College Publishing, Chapter 16 (1976).